







Even-order optical harmonics generated from centrosymmetric-material metasurfaces

Pavel Tonkaev ¹, Fangxing Lai ², Sergey Kruk, ¹ Qinghai Song ², Michael Scalora ³,
Kirill Koshelev ¹ and Yuri Kivshar ^{1,*}

¹*Nonlinear Physics Centre, Australian National University, Canberra, ACT 2601, Australia*

²*Ministry of Industry and Information Technology Key Lab of Micro-Nano Optoelectronic Information System, Guangdong Provincial Key Laboratory of Semiconductor Optoelectronic Materials and Intelligent Photonic Systems, Harbin Institute of Technology, Shenzhen 518055, People's Republic of China*

³*Aviation and Missile Center, U.S. Army CCDC, Redstone Arsenal, Alabama 35898-5000, USA*



(Received 27 March 2024; accepted 27 June 2024; published 17 July 2024)

Generation of even-order optical harmonics requires noncentrosymmetric structures being conventionally observed in crystals lacking the center of inversion. In centrosymmetric systems, even-order harmonics may arise, e.g., at surfaces but such effects are usually very weak. Here we observe optical harmonics up to fourth order generated under the normal incidence from centrosymmetric dielectric metasurfaces empowered by resonances. We design silicon metasurfaces supporting optical quasibound states in the continuum and guided-mode resonances, and demonstrate the enhancement of second-harmonic signals by over three orders of magnitude compared to nonresonant thin films. Under the optimal conditions, the brightness of the second harmonic approaches that of the third harmonic, and the fourth-order harmonic becomes detectable.

DOI: [10.1103/PhysRevResearch.6.033073](https://doi.org/10.1103/PhysRevResearch.6.033073)

I. INTRODUCTION

Generation of high-order optical harmonics is traditionally associated with plasmas and gases [1,2], but it has recently entered the realm of nanostructured solids [3–13]. Solid-state structures, unlike gases, enable efficient generation of even-order harmonics—a process reliant on the absence of inversion-point symmetry. The dominant approach toward even-order harmonic generation in nanophotonics is to employ materials with noncentrosymmetric crystalline lattices [5,14].

In nonconductive, bulk centrosymmetric media, even-order nonlinear optical processes can be triggered by several factors, including surface nonlinearities [15], strong external fields leading to inversion symmetry breaking [16–18], as well as by applying an external strain [19] or engineering internal strains by an additional overlayer [20,21]. In the presence of free electrons in the conduction band, even-order nonlinearities may be enabled by the magnetic component of the Lorentz force [22,23]. Observations of second-harmonic generation (SHG) were made in various nanoscale systems made of silicon (centrosymmetric material), including membranes [24] often enhanced by Fabry-Perot resonances [25], spherical nanoparticles [26,27] and nanowires [28,29] enhanced

by Mie resonances, photonic crystal cavities [30], as well as metasurfaces [31–33].

However, even-order effects from centrosymmetric materials are usually very weak, in sharp contrast to odd-order nonlinearities that are driven by volume nonlinear sources [34–36] (such as third-harmonic generation). Despite early observations of fourth optical harmonics from bulk silicon in 1998 [37], in nanophotonics all observations of even-order nonlinear effects discussed above have been limited to the lowest, second-order harmonic.

Here, we experimentally demonstrate generation of optical harmonics up to fourth order from resonant silicon metasurfaces driven by bound states in the continuum (BIC) and guided-mode resonances (GMR). We achieve the enhancement of the brightness of SHG, which under optimal resonant conditions approaches the brightness of third harmonic generation (THG). At resonance, we observe fourth harmonic generation (FHG) that is otherwise undetectable off resonance.

We design and fabricate metasurfaces made of amorphous silicon (a-Si) and crystalline silicon (c-Si) and compare their nonlinear properties. We characterize the metasurface's nonlinear response by pumping it in the near-IR frequency range. We observe the enhancement of over three orders of magnitude for the SHG and THG from c-Si metasurfaces driven by the GMR and BIC resonances. In contrast, the a-Si metasurface enhances SHG by two orders of magnitude. At the same time, we observe FHG from metasurfaces that support BICs. To our knowledge FHG has not been reported from silicon films or nanostructures. We also report the unexpected cubic power dependence for SHG when the pump is resonant, whereas the slope of the SHG signal approaches square dependence when the pump is tuned off resonance.

*Contact author: yuri.kivshar@anu.edu.au

Published by the American Physical Society under the terms of the [Creative Commons Attribution 4.0 International](https://creativecommons.org/licenses/by/4.0/) license. Further distribution of this work must maintain attribution to the author(s) and the published article's title, journal citation, and DOI.

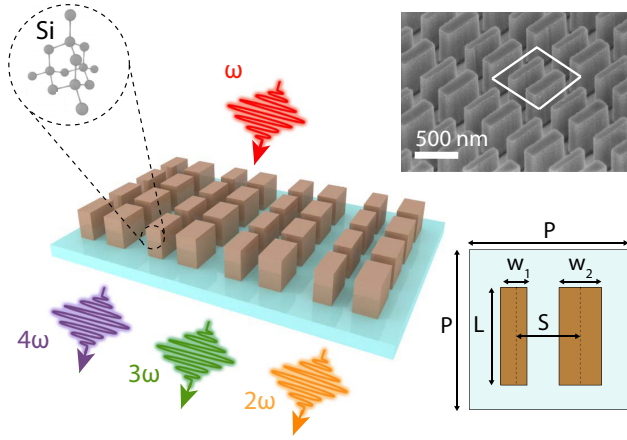


FIG. 1. Resonant metasurface for enhanced harmonic generation. A Si metasurface supporting BIC and GMR resonances for generating second to fourth optical harmonics. The inset shows a SEM image with a highlighted unit cell.

II. RESULTS AND DISCUSSION

The silicon metasurfaces are designed and fabricated to support both GMR and BIC resonances at the pump wavelength in the near-IR spectral range, with a-Si on glass and c-Si on sapphire. A schematic of the metasurfaces is shown in Fig. 1. They are composed of a square lattice of asymmetric meta-atoms consisting of bar dimers with different widths. The metasurfaces are pumped in the region from $1.4 \mu\text{m}$ to $1.75 \mu\text{m}$, with harmonics generated in the near-infrared and visible ranges. The inset provides the scanning electron microscope (SEM) image of c-Si metasurface with the unit cell highlighted. The geometrical parameters of the unit cell are bar height $h = 600 \text{ nm}$, $P = 830 \text{ nm}$, $L = 630 \text{ nm}$, $S = 380 \text{ nm}$, and $w_2 = 260 \text{ nm}$, and w_1 is varied from 180 nm to 260 nm . Parameter $\Delta w = w_2 - w_1$ is considered as an asymmetry parameter.

First, we characterize the linear transmission of c-Si metasurfaces in numerical calculations for incident polarization along the long side of the bars. We use the finite-element-method solver in COMSOL Multiphysics in the frequency domain. All calculations were realized for a metasurface placed on a semi-infinite substrate surrounded by a perfectly matched layer mimicking an infinite region. The simulation area is the unit cell extended to an infinite metasurface by using the Bloch boundary conditions. The material properties are taken from Ref. [38]. The transmission spectrum for $\Delta w = 60 \text{ nm}$ in the wavelength range from 1400 to 1800 nm and transmission map for Δw from 0 nm to 90 nm are shown in Figs. 2(a) and 2(b), respectively. The resonant features can be associated with three distinctive resonances that have wavelengths of 1580 nm , 1730 nm , and 1780 nm for $\Delta w = 60 \text{ nm}$, respectively. We focus on two modes at 1580 nm and 1730 nm , and identify their nature via calculating near-field distributions in the eigenmode solver in COMSOL Multiphysics, shown in the inset of Fig. 2(a) for $\Delta w = 60 \text{ nm}$. We can see that the mode at 1730 nm is a magnetic dipolar BIC resonance because of its distinctive asymmetric field distribution, and the mode at 1580 nm is a magnetic

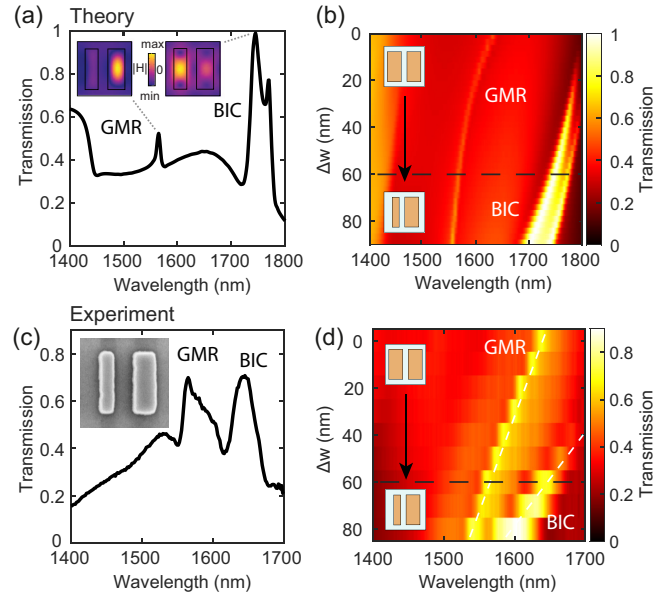


FIG. 2. Optical properties of c-Si metasurfaces. The numerically calculated (a) and measured (c) transmission spectrum of the metasurface with $\Delta w = 60 \text{ nm}$. The insets show the near-field distribution of the GMR and BIC modes, and an SEM image of the unit cell. Calculated (b) and measured (d) transmission spectra depending on the change of the asymmetric parameter Δ from an asymmetric case of 80 nm to a symmetric case of 0 nm . The black dashed lines correspond to the metasurface with $\Delta w = 60 \text{ nm}$.

dipolar GMR mode. In both modes, the volume-averaged enhancement of the local field intensity of approximately seven times is observed (see Fig. S1 in [39]).

We then measure the transmission of the c-Si metasurfaces with polarization along the long side of the bars unit cell. The transmission spectrum has two Fano-shaped features corresponding to GMR and BIC resonances. Figure 2(c) shows the transmission spectrum for the metasurfaces with $\Delta w = 60 \text{ nm}$. The inset shows the SEM image of the metasurface unit cell. Decreasing the asymmetry parameter causes both supporting resonances to display a red shift. Figure 2(d) shows the transmission spectra for c-Si metasurfaces with asymmetry parameters ranging from 0 nm to 80 nm . The BIC resonance becomes less visible with decreasing Δw , whereas the GMR mode does not change in intensity. The behavior obtained has a good agreement with theoretical prediction, which is shown in Fig. 2(b). In the case of a-Si, the spectral position of the modes is shifted to shorter wavelengths, but both modes are preserved (see Fig. S2 in [39]).

The nature of BIC and GMR modes is numerically and experimentally confirmed with their behavior for $\Delta w = 0$. More specific, the BIC mode disappears from the spectrum, while the linewidth of the GMR mode barely changes with the change of Δw , as can be seen in Figs. 2(b) and 2(d). We note that the measured resonant positions are red shifted with respect to the simulation results, and the third mode observed in numerical transmission data is not visible in the experiments. These differences can be attributed to the tolerances of fabrication and design. Also, the mode linewidth appears to be

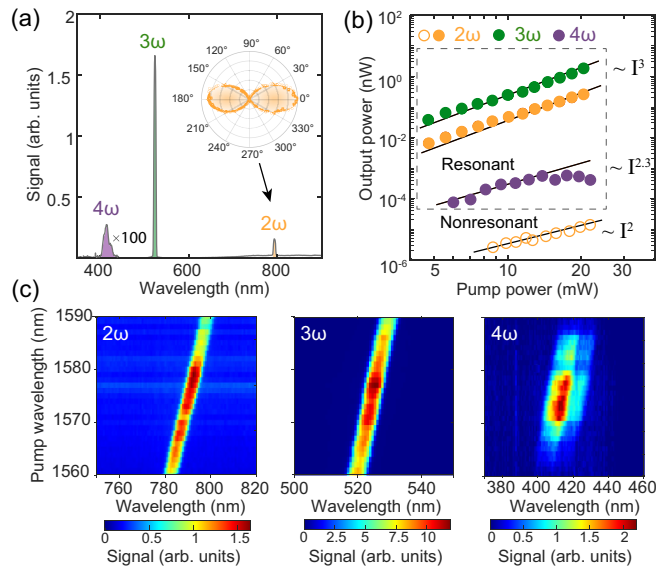


FIG. 3. Experimental harmonic generation. (a) Spectra of harmonic generation from a-Si metasurface with $\Delta w = 60$ nm supporting BIC resonance. Fourth harmonic signal is multiplied by 100. Angular dependence of second harmonic generation on pump polarization is shown on the inset with orange dots. (b) Power-power dependence for second, third, and fourth harmonics from the a-Si metasurface supporting BIC resonance, and second harmonic from the metasurface pumped nonresonantly. In the case of a resonant pump, both SHG and THG have a slope of three, whereas outside the resonance the second harmonic has a slope of two. The slope for the FHG curve equals to 2.3 for low pump intensity and decreases with the pump power increase. (c) Harmonic spectra generated by the a-Si metasurface with $\Delta w = 60$ nm for various pump wavelengths around BIC resonance. The integration time for FHG is a hundred times longer compared to SHG and THG. The fourth harmonic is observed only in the vicinity of the resonance.

larger in the experiment. This is due to the excitation source in the experiment deviating from a plane wave due to the focusing objective and a range of modes with oblique in-plane k vectors excited in the vicinity of the normal incidence.

To measure harmonic generation, we used a near-IR laser with a pulse duration of 5 ps, a repetition rate of 5.14 MHz, and a tunable wavelength in the range from 1.4 μm to 1.75 μm focused into a spot with a diameter of 25 μm . The signals are collected in transmission by an objective lens with NA 0.42 (see Fig. S3 in [39] for more details). Figure 3(a) shows the spectrum of harmonic generation from the a-Si metasurface with $\Delta w = 60$ nm pumped resonantly at the wavelength of 1575 nm and with the peak power density of 3 $\text{GW} \cdot \text{cm}^{-2}$. A SHG signal is observable at 788 nm, while THG is observed at 525 nm. We remark that the magnitude of the SHG signal is one order of magnitude smaller than the magnitude of the THG signal. While this may seem unusual, the relative magnitudes of the generated harmonics are sensitive to pump tuning with respect to resonance peak, as well as material dispersion and polarization. Under ordinary circumstances, in a cavity environment it is also possible for SHG maxima to be shifted relative to THG maxima. The inset of Fig. 3(a) demonstrates

that the normalized SHG signal depends on the angle of pump polarization, where 0° corresponds to polarization coinciding with the longest side of the bars. In the case of pump polarization orthogonal to the bars, the SH signal is significantly smaller. The same pattern is observed for THG (see Fig. S4 in [39]). The polarimetry of the THG and SHG signals reveals that both harmonics pumped at the BIC resonance preserve the polarization of the excitation and the degrees of polarization are 0.8 and 0.7, respectively. We note that FHG can also be observed in the spectrum at the wavelength of 415 nm. Figure 3(c) shows the harmonic spectra recorded for the various pump wavelengths around BIC resonance. The FHG is observed only in the vicinity of the BIC resonance, whereas the SHG and THG are observed outside the resonant pump.

We also record the power dependence of SHG, THG, and FHG pumped resonantly at the wavelength of 1636 nm, which corresponds to the BIC resonance of the metasurface. The dependencies for SHG, THG, and FHG are indicated in Fig. 3(b) with orange, green, and purple circles, respectively. Both THG and SHG curves agree well with the cubic power law. The results recorded for the same metasurface, but pumped at a wavelength of 1470 nm, which excites the GMR mode of the structure, exhibit similar behavior. The slope of the FHG curve is less than the expected quadratic dependence, and it equals 2.3 for low pump intensity and decreases as pump power increases. When the pump is nonresonant, the situation changes for SHG. The signal shown in Fig. 3(b) is denoted by the hollow circles, and shows good agreement with the quadratic power law. In contrast, THG preserves the same slope of three even when the pump is tuned outside the resonance (see Fig. S5 in [39]). The results for the reference c-Si and a-Si unstructured films also show slopes two and three for the SHG and THG, respectively. The generation of the second harmonic with a slope larger than two has previously been observed in semiconductors [40,41] and hybrid structures [42,43]. That behavior is caused by the generation of the static electric field by the high-intensity laser beam.

To study the dependence of the SHG and THG on asymmetry parameter and pump wavelength, we measure the harmonic signal from the metasurfaces having different asymmetries, and pump wavelengths from 1400 nm to 1750 nm. The maximum SHG and THG values are determined and normalized by the harmonic signal generated by a similar silicon film. The enhancement values obtained for a-Si metasurface are shown in Figs. 4(a) and 4(b). The maximum enhancement for SHG is three orders of magnitude, whereas it is about two orders of magnitude for THG. The BIC mode is clearly observed in both second and third harmonics enhancement maps, and is in good agreement with mode positions in the linear spectra. Figure 4(c) sums up the enhancement for SHG (orange circles) and THG (green circles). Both SHG and THG enhanced by the BIC tend to be larger than the signals enhanced by the GMR modes.

For c-Si metasurfaces the positions of the enhancement are shifted compared to the a-Si metasurfaces, similar to the linear spectra features shift. Figures 4(d) and 4(e) demonstrate the enhancement from c-Si metasurfaces depending on asymmetry parameter and pump wavelength. In contrast with a-Si metasurfaces, both modes are clearly distinguishable for SHG

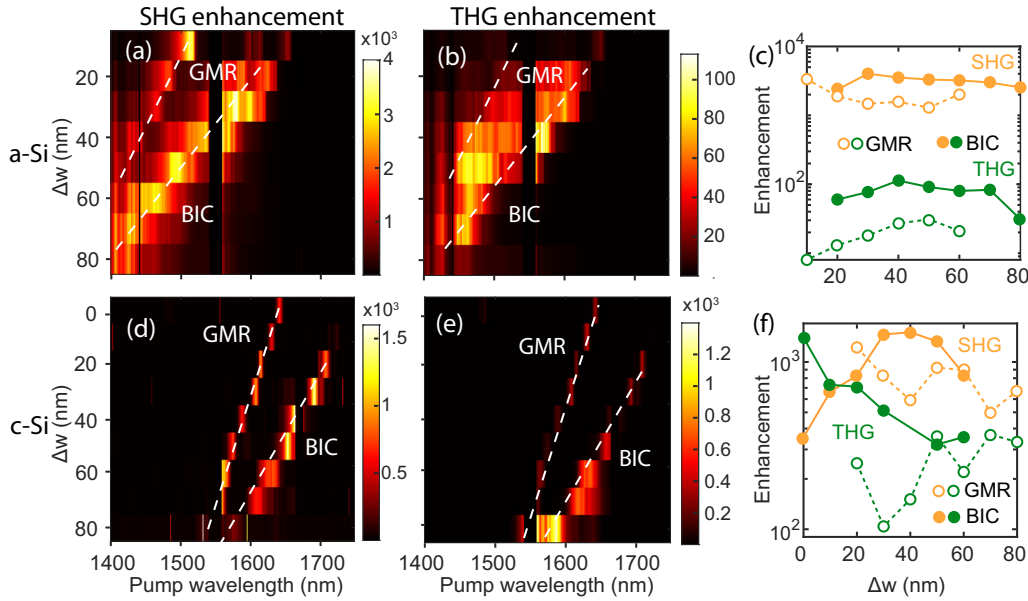


FIG. 4. Harmonic enhancement for a-Si and c-Si metasurfaces. Second harmonic enhancement from (a) a-Si and (d) c-Si dependence on asymmetric parameter and pump wavelength. (c) Maximum of second and third harmonic enhancement for different modes depending on the asymmetric parameter for a-Si metasurface. Third harmonic generation enhancement from (b) a-Si and (e) c-Si dependence on asymmetric parameter and pump wavelength. (f) Maximum of second and third harmonics enhancement for different modes depending on the asymmetric parameter for c-Si metasurface.

and THG enhancement maps. SH and TH signal enhancements are about three orders of magnitude. SH enhancement is compared to the best case scenario where the wave is incident at approximately 70 degrees [25]. A decrease in the asymmetry parameter causes the decrease of linewidth for the BIC mode and its eventual disappearance from the spectrum for the fully symmetric case. The enhancement of SHG and THG are summarized in Fig. 4(f) by the orange and green circles, respectively. We note that, meanwhile, the SHG enhancement is in the same order of magnitude for a-Si and c-Si metasurfaces, and the SHG signal from the c-Si metasurfaces is one order of magnitude lower than the SHG from the a-Si metasurface (see Fig. S6 in [39])

As noted earlier, we also observe the fourth harmonic generation. Since a-Si metasurfaces have modes at around 1350 nm for $\Delta w = 80$ nm to 1650 nm for $\Delta w = 10$ nm according to the linear transmission spectra, the spectral position of the fourth harmonic is located either just outside or at the edge of the spectrometer's range. Thus, it can be detected only for the BIC resonance for the a-Si metasurfaces with size parameters that yield near-symmetric structures. However, for those size parameters, the BIC resonance is either weak or not observed. In contrast, c-Si metasurfaces have modes that are spectrally redshifted and enable the observation of the fourth harmonic within the spectrometer spectral range. However, the harmonics themselves are weaker for the c-Si, which complicates their observation.

There are several mechanisms proposed to explain the symmetry breaking in silicon that leads to even harmonic generation. Since there is no proper band structure at the interface, nonlocal effects contribute to surface and quadrupolar

bulk SHG [44]. An intense pump laser pulse causes weak direct-current static electric field that affects the phases of the optical field half-cycles and breaks the symmetry, producing even harmonics in silicon [45,46]. Inhomogeneous laser fields in the vicinity of plasmonic resonances can also produce even harmonics [47]. This scenario might be relevant for strongly excited semiconductors, but this issue is beyond the scope of this work.

Even harmonics may be triggered by a combination of surface and magnetic terms [24,25,48]. For example, the bound electron term $(\mathbf{P}_\omega \cdot \nabla)\mathbf{E}_\omega$ and the magnetic term $\mathbf{J}_\omega \times \mathbf{H}_\omega$ are the dominant second harmonic sources. Here, polarization, current, and fields are to be interpreted as envelope functions at the given frequency. Similarly, fourth harmonic nonlinear surface and magnetic sources may also be derived and written as $(\mathbf{P}_{2\omega} \cdot \nabla)\mathbf{E}_{2\omega}$ and $\mathbf{J}_{2\omega} \times \mathbf{H}_{2\omega}$. However, efficient third harmonic generation activates additional surface and magnetic terms that are proportional to $(\mathbf{P}_{3\omega} \cdot \nabla)\mathbf{E}_\omega$, $\mathbf{J}_{3\omega} \times \mathbf{H}_\omega$, and $\mathbf{J}_\omega \times \mathbf{H}_{3\omega}$, as well as fourth order bulk terms proportional to $\chi^{(3)}E_{3\omega}E_\omega$. Therefore, there is some expectation that fourth harmonic generation will fall within the range of parameters that determine a combination of second and third harmonic generation. Currently, while the theory can provide good guidance, we do not have a clear theoretical framework for the quantitative aspects of our observations.

III. CONCLUSION

In summary, we have studied optical harmonic generation from metasurfaces made of amorphous and crystalline silicon. We have observed the generation of the second and third

harmonics enhanced by at least three orders of magnitude via GMR and BIC resonances in the near-IR range. This enabled significant generation of the fourth harmonics at the BIC resonance. We have observed the deviation in the power laws for both even harmonics at the BIC resonance. We believe that our results reveal that dielectric metasurfaces made of centrosymmetric materials can exhibit generally unexpectedly strong even-order nonlinear effects when they are empowered by high- Q optical resonances associated with the bound states in the continuum.

ACKNOWLEDGMENTS

The authors thank C. Cojocaru, S. A. Maier, N. C. Panoiu, J. Trull, and M. A. Vincenti for useful discussions and suggestions. This work was supported by the Australian Research Council (Grants No. DP210101292 and No. DE210100679), the International Technology Center Indo-Pacific (ITC IPAC) via Army Research Office (Contract No. FA520923C0023), and the National Natural Science Foundation of China (Grants No. 12334016, No. 12025402, and No. 12261131500).

-
- [1] N. H. Burnett, H. A. Baldis, M. C. Richardson, and G. D. Enright, Harmonic generation in CO₂ laser target interaction, *Appl. Phys. Lett.* **31**, 172 (1977).
- [2] M. Ferray, A. L'Huillier, X. F. Li, L. A. Lompre, G. Mainfray, and C. Manus, Multiple-harmonic conversion of 1064 nm radiation in rare gases, *J. Phys. B: At. Mol. Opt. Phys.* **21**, L31 (1988).
- [3] G. Vampa, B. G. Ghamsari, S. Siadat Mousavi, T. J. Hammond, A. Olivieri, E. Lisicka-Skrek, A. Y. Naumov, D. M. Villeneuve, A. Staudte, P. Berini, and P. B. Corkum, Plasmon-enhanced high-harmonic generation from silicon, *Nat. Phys.* **13**, 659 (2017).
- [4] H. Liu, C. Guo, G. Vampa, J. L. Zhang, T. Sarmiento, M. Xiao, P. H. Bucksbaum, J. Vučković, S. Fan, and D. A. Reis, Enhanced high-harmonic generation from an all-dielectric metasurface, *Nat. Phys.* **14**, 1006 (2018).
- [5] M. R. Shcherbakov, H. Zhang, M. Tripepi, G. Sartorello, N. Talisa, A. AlShafey, Z. Fan, J. Twardowski, L. A. Krivitsky, A. I. Kuznetsov, E. Chowdhury, and G. Shvets, Generation of even and odd high harmonics in resonant metasurfaces using single and multiple ultra-intense laser pulses, *Nat. Commun.* **12**, 1 (2021).
- [6] D. Zhang, Y. Tu, H. Wu, Z. Lyu, Z. Zhao, and J. Yuan, Enhanced high harmonic and terahertz generation from linbo 3 metasurface, in *2021 46th International Conference on Infrared, Millimeter and Terahertz Waves (IRMMW-THz)* (IEEE, 2021), pp. 1–2.
- [7] C. P. Schmid, L. Weigl, P. Grössing, V. Junk, C. Gorini, S. Schlauderer, S. Ito, M. Meierhofer, N. Hofmann, D. Afanasiev, J. Crewse, K. A. Kokh, O. E. Tereshchenko, J. Gütde, F. Evers, J. Wilhelm, K. Richter, U. Höfer, and R. Huber, Tunable non-integer high-harmonic generation in a topological insulator, *Nature (London)* **593**, 385 (2021).
- [8] J.-K. An and K.-H. Kim, Efficient non-perturbative high-harmonic generation from nonlinear metasurfaces with low pump intensity, *Opt. Laser Technol.* **135**, 106702 (2021).
- [9] V. Zubyyuk, L. Carletti, M. Shcherbakov, and S. Kruk, Resonant dielectric metasurfaces in strong optical fields, *APL Mater.* **9**, 060701 (2021).
- [10] G. Zograf, K. Koshelev, A. Zalogina, V. Korolev, R. Hollinger, D.-Y. Choi, M. Zuerch, C. Spielmann, B. Luther-Davies, D. Kartashov, S. V. Makarov, S. S. Kruk, and Y. Kivshar, High-harmonic generation from resonant dielectric metasurfaces empowered by bound states in the continuum, *ACS Photonics* **9**, 567 (2022).
- [11] S. D. R. Abbing, R. Kolkowski, Z.-Y. Zhang, F. Campi, L. Lötgering, A. F. Koenderink, and P. M. Kraus, Extreme-ultraviolet shaping and imaging by high-harmonic generation from nanostructured silica, *Phys. Rev. Lett.* **128**, 223902 (2022).
- [12] A. Zalogina, L. Carletti, A. Rudenko, J. V. Moloney, A. Tripathi, H.-C. Lee, I. Shadrivov, H.-G. Park, Y. Kivshar, and S. S. Kruk, High-harmonic generation from a subwavelength dielectric resonator, *Sci. Adv.* **9**, eadg2655 (2023).
- [13] P. Jangid, F. U. Richter, M. L. Tseng, I. Sinev, S. Kruk, H. Altug, and Y. Kivshar, Spectral tuning of high-harmonic generation with resonance-gradient metasurfaces, *Adv. Mater.* **36**, 2307494 (2024).
- [14] S. Liu, P. P. Vabishchevich, A. Vaskin, J. L. Reno, G. A. Keeler, M. B. Sinclair, I. Staude, and I. Brener, An all-dielectric metasurface as a broadband optical frequency mixer, *Nat. Commun.* **9**, 1 (2018).
- [15] D. Timbrell, J. W. You, Y. S. Kivshar, and N. C. Panoiu, A comparative analysis of surface and bulk contributions to second-harmonic generation in centrosymmetric nanoparticles, *Sci. Rep.* **8**, 3586 (2018).
- [16] A. Bouhelier, M. Beversluis, A. Hartschuh, and L. Novotny, Near-field second-harmonic generation induced by local field enhancement, *Phys. Rev. Lett.* **90**, 013903 (2003).
- [17] E. Timurdogan, C. V. Poulton, M. J. Byrd, and M. R. Watts, Electric field-induced second-order nonlinear optical effects in silicon waveguides, *Nat. Photonics* **11**, 200 (2017).
- [18] K.-T. Lee, M. Taghinejad, J. Yan, A. S. Kim, L. Raju, D. K. Brown, and W. Cai, electrically biased silicon metasurfaces with magnetic mie resonance for tunable harmonic generation of light, *ACS Photonics* **6**, 2663 (2019).
- [19] C. Schriever, C. Bohley, and R. B. Wehrspohn, Strain dependence of second-harmonic generation in silicon, *Opt. Lett.* **35**, 273 (2010).
- [20] M. Cazzanelli, F. Bianco, E. Borga, G. Pucker, M. Ghulinyan, E. Degoli, E. Luppi, V. Véniard, S. Ossicini, D. Modotto, S. Wabnitz, R. Pierobon, and L. Pavesi, Second-harmonic generation in silicon waveguides strained by silicon nitride, *Nat. Mater.* **11**, 148 (2012).
- [21] Y. Zhao, W. Jia, X.-J. Wang, Y. Dong, H.-H. Fang, Y. Yang, and H.-B. Sun, Second-harmonic generation in strained silicon metasurfaces, *Adv. Photonics Res.* **3**, 2200157 (2022).
- [22] Z. Guo, Z. Li, and K. Guo, The enhanced second-harmonic generation based on magnetic-Lorentz-force effect, *Ann. Phys.* **531**, 1800470 (2019).
- [23] G. Yang, Z. Li, Q. Kang, K. Guo, H. Zhang, and Z. Guo, Enhanced magnetic Lorentz force second harmonic generation

- originating from a double-resonances plasmonic metasurface, *J. Phys. D: Appl. Phys.* **54**, 175110 (2021).
- [24] M. Scalora, J. Trull, C. Cojocaru, M. A. Vincenti, L. Carletti, D. de Ceglia, N. Akozbek, and C. De Angelis, Resonant, broadband, and highly efficient optical frequency conversion in semiconductor nanowire gratings at visible and UV wavelengths, *J. Opt. Soc. Am. B* **36**, 2346 (2019).
- [25] K. A. Hallman, L. Rodríguez-Suné, J. Trull, C. Cojocaru, M. A. Vincenti, N. Akozbek, R. Vilaseca, and M. Scalora, Harmonic generation from silicon membranes at visible and ultraviolet wavelengths, *Opt. Express* **31**, 792 (2023).
- [26] S. V. Makarov, M. I. Petrov, U. Zywiets, V. Milichko, D. Zuev, N. Lopanitsyna, A. Kuksin, I. Mukhin, G. Zograf, E. Ubyivovk, D. A. Smirnova, S. Starikov, B. N. Chichkov, and Y. S. Kivshar, Efficient second-harmonic generation in nanocrystalline silicon nanoparticles, *Nano Lett.* **17**, 3047 (2017).
- [27] D. Smirnova, A. I. Smirnov, and Y. S. Kivshar, Multipolar second-harmonic generation by Mie-resonant dielectric nanoparticles, *Phys. Rev. A* **97**, 013807 (2018).
- [28] P. R. Wiecha, A. Arbouet, H. Kallel, P. Periwal, T. Baron, and V. Paillard, Enhanced nonlinear optical response from individual silicon nanowires, *Phys. Rev. B* **91**, 121416 (2015).
- [29] P. R. Wiecha, A. Arbouet, C. Girard, T. Baron, and V. Paillard, Origin of second-harmonic generation from individual silicon nanowires, *Phys. Rev. B* **93**, 125421 (2016).
- [30] M. Galli, D. Gerace, K. Welna, T. F. Krauss, L. O'Faolain, G. Guizzetti, and L. C. Andreani, Low-power continuous-wave generation of visible harmonics in silicon photonic crystal nanocavities, *Opt. Express* **18**, 26613 (2010).
- [31] J. Bar-David and U. Levy, Nonlinear diffraction in asymmetric dielectric metasurfaces, *Nano Lett.* **19**, 1044 (2019).
- [32] J. Xu, E. Plum, V. Savinov, and N. I. Zheludev, Second harmonic generation in amorphous silicon-on-silica metamaterial, *APL Photonics* **6**, 036110 (2021).
- [33] J. T. Wang, P. Tonkaev, K. Koshelev, F. Lai, S. Kruk, Q. Song, Y. Kivshar, and N. C. Panoiu, Resonantly enhanced second- and third-harmonic generation in dielectric nonlinear metasurfaces, *Opto Electron. Adv.* **7**, 230186 (2024).
- [34] P. Guyot-Sionnest, W. Chen, and Y. R. Shen, General considerations on optical second-harmonic generation from surfaces and interfaces, *Phys. Rev. B* **33**, 8254 (1986).
- [35] J. E. Sipe, D. J. Moss, and H. M. van Driel, Phenomenological theory of optical second- and third-harmonic generation from cubic centrosymmetric crystals, *Phys. Rev. B* **35**, 1129 (1987).
- [36] Y. R. Shen, Surface contribution versus bulk contribution in surface nonlinear optical spectroscopy, *Appl. Phys. B* **68**, 295 (1999).
- [37] Y.-S. Lee and M. C. Downer, Reflected fourth-harmonic radiation from a centrosymmetric crystal, *Opt. Lett.* **23**, 918 (1998).
- [38] H. H. Li, Refractive index of silicon and germanium and its wavelength and temperature derivatives, *J. Phys. Chem. Ref. Data* **9**, 561 (1980).
- [39] See Supplemental Material at <http://link.aps.org/supplemental/10.1103/PhysRevResearch.6.033073> for (Fig. S1) numerically calculated electric field enhancement in meta-atom, (Fig. S2) transmission spectra for a-Si metasurfaces, (Fig. S3) experimental setup schematics, (Fig. S4) angles dependence of third harmonic generation on pump polarization, (Fig. S5) power dependence of third harmonic from metasurface outside the resonance, and (Fig. S6) harmonics spectrum from the c-Si metasurfaces.
- [40] V. Fomenko, J.-F. Lami, and E. Borguet, Nonquadratic second-harmonic generation from semiconductor-oxide interfaces, *Phys. Rev. B* **63**, 121316 (2001).
- [41] W. Wang, G. Lüpke, M. D. Ventra, S. T. Pantelides, J. M. Gilligan, N. H. Tolk, I. C. Kizilyalli, P. K. Roy, G. Margaritondo, and G. Lucovsky, Coupled electron-hole dynamics at the Si/SiO₂ interface, *Phys. Rev. Lett.* **81**, 4224 (1998).
- [42] X. Wen, W. Xu, W. Zhao, J. B. Khurgin, and Q. Xiong, Plasmonic hot carriers-controlled second harmonic generation in WSe₂ bilayers, *Nano Lett.* **18**, 1686 (2018).
- [43] Y. Sun, A. Larin, A. Mozharov, E. Ageev, O. Pashina, F. Komissarenko, I. Mukhin, M. Petrov, S. Makarov, P. Belov, and D. Zuev, All-optical generation of static electric field in a single metal-semiconductor nanoantenna, *Light: Sci. Appl.* **12**, 1 (2023).
- [44] N. Tancogne-Dejean, C. Giorgetti, and V. Véniard, *Ab initio* description of second-harmonic generation from crystal surfaces, *Phys. Rev. B* **94**, 125301 (2016).
- [45] T. Apostolova and B. Obreshkov, High harmonic generation in crystalline silicon irradiated by an intense ultrashort laser pulse, *Eur. Phys. J. D* **75**, 267 (2021).
- [46] A. V. Ovchinnikov, O. V. Chefonov, E. D. Mishina, and M. B. Agranat, Second harmonic generation in the bulk of silicon induced by an electric field of a high power terahertz pulse, *Sci. Rep.* **9**, 9753 (2019).
- [47] M. F. Ciappina, J. Biegert, R. Quidant, and M. Lewenstein, High-order-harmonic generation from inhomogeneous fields, *Phys. Rev. A* **85**, 033828 (2012).
- [48] S. Mukhopadhyay, L. Rodríguez-Suné, C. Cojocaru, M. A. Vincenti, K. Hallman, G. Leo, M. Belchovski, D. de Ceglia, M. Scalora, and J. Trull, Three orders of magnitude enhancement of second and third harmonic generation in the visible and ultraviolet ranges from plasmonic gold nanogratings, *APL Photonics* **8**, 046108 (2023).